Noura Mossaed Saleh*, Hisham Fouad Aly, Eman Abdelrahman Mahmoud Ahmed and Refaat Mohamed Mahfouz

Dehydration of un-irradiated and gamma and electron-beam irradiated europium acetate hydrate under non-isothermal conditions: kinetics of the dehydration process of un-irradiated material

https://doi.org/10.1515/ract-2024-0317
Received June 10, 2024; accepted November 27, 2024;
published online December 24, 2024

Abstract: The authors present here the decomposition of un-irradiated (pristine) as well as of gamma (γ) and electron beam (EB) irradiated samples of europium (III) acetate hydrate ($EuAc.xH_2O$) in the temperature range of 25–900 °C in the air atmosphere. Two absorbed doses of 10^3 (γ-ray) and 10^2 kGy (EB) were examined. The profiles of the TG curves of the dehydration process display noticeable changes in induction periods and mass loss percentages by exposure to irradiation. The kinetics of the dehydration process were analyzed using both model-fitting and model-free approaches. The dehydration process was controlled by the phase boundary model (R_2). The E_a –α plots indicate that the dehydration is not a complex process and follows one reaction mechanism. Powder X-ray diffraction displayed that europium acetate hydrate crystallizes in a monoclinic system *(SG P2/m)*, and no phase transformation was detected by two sources of irradiation up to 10^3 (γ-ray) and 10^2 kGy (EB). Thermodynamic parameters of the dehydration process were calculated and assessed. A predicted thermogram (TG) of the isothermal dehydration of $EuAc.xH_2O$ was constructed from non-isothermal data and used to determine the reaction model and the kinetic parameters of the dehydration process.

***Corresponding author: Noura Mossaed Saleh**, Chemistry Department, Faculty of Science, Assiut University, 71516, Assiut, Egypt,
E-mail: nouramossaed@aun.edu.eg
Hisham Fouad Aly, Egyptian Atomic Energy Authority, Cairo, Egypt
Eman Abdelrahman Mahmoud Ahmed, Egyptian Petroleum Research Institute, Cairo, Egypt
Refaat Mohamed Mahfouz, Chemistry Department, Faculty of Science, Assiut University, 71516, Assiut, Egypt

Keywords: gamma irradiation; electron beam irradiation; non-isothermal dehydration; isoconversional approach; europium acetate hydrate

1 Introduction

The thermal properties of inorganic materials are significantly affected by ionizing radiation (X-rays or γ-rays).[1] Previous investigations carried out by our research group concerning the thermal decomposition of metal acetylacetonates and acetates demonstrated that substantial alterations in the thermal decomposition characteristics could result from pre-exposure to both indirect and direct ionizing radiation. An increase in the absorbed dose by a substance generally results in modifications in the reaction mechanism and thermodynamic parameters of the decomposition process, as well as a reduction in the induction period.[2–5] Rare earth acetylacetonates and acetates exhibit considerable potential as precursors to rare earth oxide nanoparticles, which are utilized in industrial and technical applications.

It has been found that isoconversional methods offer several advantages over model-fitting approaches and could potentially account for the discrepancy in apparent activation energies that arise from the conversion degree, α, or the dependence of E_a –α.[6,7] Model-free approaches to calculate the values of E_a are supported by nonlinear and linear isoconversional methods, which operate on the premise that the rate of a solid-state reaction, α, is solely determined by temperature. Thermally stimulated solid-state reactions are an intrinsically multi-step process for which the apparent activation energy, E_a, is varied with the conversion degree, α. Even if E_a shows a constant value, there is still a possibility that many intrinsic reactions have nearly similar kinetic barriers, and the overall kinetics is determined by a single stage.[8–10] Thermal investigations about lanthanide acetates were primarily concerned with identifying the gaseous byproducts and evaluating the characteristics and stability

of the intermediates; the mechanisms and kinetics of the thermal decomposition reactions were not further clarified.[11] We present in this work the initial phase of our investigation on the thermal dehydration of $Eu(CH_3COO)_3.xH_2O$; our purpose was as follows:

a) Radiation-induced impacts on the thermal behaviour and phase transformation of $EuAc.xH_2O$.
b) Kinetics investigations of the thermal dehydration of pristine $EuAc.xH_2O$ by using nonlinear and linear isoconversional methods.

2 Materials and methods

2.1 Materials

The formula for Europium (III) acetate hydrate (99.9 %) is as follows:

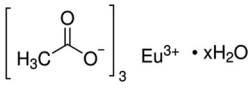

(Or shortly $EuAc.xH_2O$) was obtained commercially from Alfa Aesar and was utilized without additional purification.

2.2 Experimental methods

Thermogravimetry (TG) experiments were conducted on the model TGA Q50 V20.13 Build 39 thermal analyzer (EGA/U.S.A.). Every experiment is conducted in an air-filled atmosphere. 40 mL/min was the rate of flow. The heating rates utilized in this experiment were dynamic (non-isothermal): 5, 10, and 12.5 °C/min. It was observed that the data displayed overlaps when duplicate runs were performed under identical conditions, which indicates that the reproducibility was satisfactory. On a Philips Model PW1710 utilizing CuKα radiation (λ = 1.54 Å) and operating at 30 mA, P-XRD patterns were recorded. The continuous speed of the scan mode was 0.06 deg/min.

Irradiations by gamma rays and electron beams were conducted at the Egyptian Atomic Energy Authority (EAEA), National Centre for Radiation Research and Technology (NCRRT), located in Cairo, Egypt. To irradiate the sample with electron beams, a 25 kW electron accelerator with a magnitude of 1.5 MeV was utilized. The speed of the conveyor was modified by 20 mm/min. The dose rate was determined by employing the FWT-60-00 dosimeter, which had undergone calibration using the Ceric/Cerous dosimeter. To subject the samples to γ-ray irradiation, they were vacuum-encapsulated in glass vials and subjected to continuous radiation exposure via a Co-60 γ-ray source. A dosage rate of 1.3 kGy/h was utilized in all irradiation experiments conducted at a temperature of 25 °C. Precise adjustments were achieved to the absorbed doses in the irradiated samples by utilizing the mass attenuation and energy absorption coefficients for both the sample and the dosimeter solutions. This was done after the absorbed dose had been attenuated and the source had been calibrated against a Fricke ferrous sulfate dosimeter by ASTM standard practice E 1026-13.[12] KBr pellets were subjected to transmission mode FT-IR analysis within the wavenumber of 4,000–400 cm^{-1}.

2.3 Mathematical methods

2.3.1 Kinetic calculations

Incongruent dissociative vaporization results in the formation of a gaseous product C(g) and a solid product B(s), which describes the non-isothermal dehydration of $EuAc.xH_2O$.

$$A(s) \rightarrow B(s) + C(g)$$

The solid product that results from a solid reactant transformation exhibits significant differences in both crystal structure and morphology. This is evident in the formation of conglomerates consisting of separated nanoparticles of product, which are nearly “transparent” in the case of an exhaust flow containing different gas products generated during thermal decomposition reactions.[13]

Equation (1) was utilized for calculating the conversion degree, α.

$$a = \frac{m_o - m_T}{m_o - m_f} \tag{1}$$

Where m_f, m_T, and m_0 are the final, current, and initial sample mass at the temperature T, respectively.

The basic equations of the isoconversional model used in this work were reported in our previous publication.[5]

The following linear isoconversional methods, namely, *Flynn-Wall-Ozawa (FWO), Kissinger-Akahira-Sunose (KAS), Tang, and Iterative* equations (equations (2)–(5), respectively),[14–23] were applied in this work.

$$\ln \beta = \ln \frac{AE_a}{Rg(a)} - 5.3305 - 1.052\frac{E_a}{RT} \tag{2}$$

where E_a denotes the apparent activation energy, $Jmol^{-1}$, A denotes the pre-exponential factor, s^{-1}, T is absolute temperature, K, β is the heating rate, Ks^{-1}, $g(a)$ is the integral

function of conversion, and R is the gas constant, 8.314 J mol^{-1} K^{-1}.

$$\ln\left(\frac{\beta}{T^2}\right) = \ln\frac{AR}{E_a g(\alpha)} - \frac{E_a}{RT} \quad (3)$$

$$\ln\frac{\beta}{T^{1.894661}} = \left(\ln\frac{AE_{a\alpha}}{Rg(\alpha)} + 3.63504095 - 1.89466100\ln E_{a\alpha}\right) - 1.00145033\frac{E_{a\alpha}}{RT} \quad (4)$$

$$\ln\left(\frac{\beta}{h(x)T^2}\right) = \ln\frac{AR}{E_a g(\alpha)} - \frac{E_a}{RT} \quad (5)$$

where h(x) is expressed by the *fourth Senum and Yang approximation formulae*[24]

$$h(x) = \frac{x^4 + 18x^3 + 88x^2 + 96x}{x^4 + 20x^3 + 120x^2 + 240x + 120} \quad (6)$$

The temperature integral (Px) was approximated based on *Doly's and the Coats-Redfern* approximations[25,26] for *FWO* and *KAS* methods. *Tang* et al. method utilizes the following approximation.

$$P(x) = \frac{\exp(-x)}{x} \cdot \frac{1}{1.00198882x + 1.87391198} \quad (7)$$

For a constant conversion, the data acquired at different heating rates should be employed in the generation of linear trends that depict the correlation between the left-hand side of each equation and 1/T. The slope of these lines should be proportional in a direct manner to the respective values of 1.052 E_a R, E_a/R, 1.00145033 E_a/R, and E_a/R. The E_a values were determined through the experimental data numerical fitting utilizing the least-square fitting procedure integrated into the *MATLAB 2015* software.

The *Friedman method*, which permits the determination of the activation energy without any information or assumptions concerning the reaction model or temperature integral, is the most frequently employed isoconversional differential method.

$$\ln\left(\frac{d\alpha}{dt}\right) = \ln f(\alpha) + \ln A_\alpha - \frac{E_a}{RT} \quad (8)$$

where t is the time (min), α is the conversion degree, and $f(\alpha)$ is the conversion function dependent on the reaction mechanism. Table 1 contains a compilation of reaction models utilized in solid-state reactions.

By plotting the left-hand side of equation (8), ln(dα/dt), against 1/T, it is possible to derive linear fittings for points undergoing the same conversion degree. Determining the activation energy at a certain conversion is possible by examining the corresponding line slope.[27–29]

Table 1: Reaction models used in this work.

Symbol	Reaction model	$f(\alpha)$	$g(\alpha)$
D_1	One dimensional diffusion	$1/2\alpha$	α^2
D_2	Two-dimensional diffusion (bidimentional particle shape) Valensi equation	$1/[-\ln(1-\alpha)]$	$(1-\alpha)\ln(1-\alpha)+\alpha$
D_3	Three-dimensional diffusion (tridimentional particle shape) Jander equation	$3(1-\alpha)^{1/3}/2[(1-\alpha)^{-1/3}-1]$	$[1-(1-\alpha)^{1/3}]^2$
A_2	Avrami-Erofeev(n = 2)	$2(1-\alpha)[-\ln(1-\alpha)]^{1/2}$	$[-\ln(1-\alpha)]^{1/2}$
A_3	Avrami-Erofeev(n = 3)	$3(1-\alpha)[-\ln(1-\alpha)]^{2/3}$	$[-\ln(1-\alpha)]^{1/3}$
A_4	Avrami-Erofeev(n = 4)	$4(1-\alpha)[-\ln(1-\alpha)]^{3/4}$	$[-\ln(1-\alpha)]^{1/4}$
F_1	First-order (Mampel)	$(1-\alpha)$	$-\ln(1-\alpha)$
R_2	Phase-boundary controlled reaction(contracting area, i.e., bidimensional shape)	$2(1-\alpha)^{1/2}$	$[1-(1-\alpha)^{1/2}]$
R_3	Phase-boundary controlled reaction(contracting volume, i.e.,tridimensional shape)	$3(1-\alpha)^{2/3}$	$[1-(1-\alpha)^{1/3}]$

Due to the inherent complexity of solid state reaction processes as a whole,[30] this study utilized two kinetic methods in tandem to process the DTG data and compute the Arrhenius parameters, including the pre-exponential factor (A) for the dehydration step and the activation energy (E_a). The following describe these methods:

Kissinger equation:[16]

$$\ln\left(\frac{\beta}{T_m^2}\right) = \ln\frac{AR}{E_a} - \frac{E_a}{RT_m} \quad (9)$$

where T_m is the maximum peak temperature

Ozawa–Flynn–Wall equation:[31]

$$\ln\beta = \ln\left(\frac{AE_a}{Rg(\alpha)}\right) - 2.315 - 0.4567\frac{E_a}{RT_m} \quad (10)$$

2.3.2 Study of the thermal dehydration mechanism

2.3.2.1 Master plots based on the integral form of the kinetic data

To evaluate the reaction mechanism, the kinetic data were analyzed employing the *master plots* method with the equation provided below.[32]

$$\frac{P(x)}{P(x_{0.5})} = \frac{g(\alpha)}{g(0.5)} \quad (11)$$

where $x_{0.5} = E_a/(RT_{0.5})$, $T_{0.5}$ is the temperature required to obtain a 0.5 conversion degree (α = 0.5).

Equation (11) consists of the experimental data on its left side and different equations representing theoretical models on its right side.[5]

2.3.2.2 Málek's equations

The Málek equations were utilized in the current study to determine the most suitable kinetic model. Equation (13) can be derived from the rearrangement of equation (12) to facilitate further evaluation of the special function y(α).[33–35]

$$\frac{d\alpha}{dt} = A\exp\left(\frac{-E_a}{RT}\right)f(\alpha) \tag{12}$$

$$y(\alpha) = \frac{d\alpha}{dt}e^{\frac{E_a}{RT}} = Af(\alpha) \tag{13}$$

The $z(\alpha)$ function is introduced to formulate as

$$z(\alpha) = f(\alpha)g(\alpha) = P(x)\frac{d\alpha}{dt}^{*}\frac{T}{\beta} \tag{14}$$

Equations (13) and (14) demonstrate that the E_a value must be known under non-isothermal conditions. By plotting the dependence of y(α) and z(α), normalized with the values 0–1, the reaction model type can be identified by calculating the maximal values, including α_p, α_m, and α_p^{∞} observed from the plots between dα/dt, $y(\alpha)$, and $z(\alpha)$ functions versus α, respectively.

The mathematical properties of the y(α) and z(α) functions of fundamental kinetic models are succinctly outlined in Table 2.[36,37]

2.3.2.3 Determination of the most probable mechanism function

The estimation of the most correct reaction mechanism was performed utilizing the subsequent equation, i.e., the $g(\alpha)$ function :[22]

$$ln\,g(\alpha) = \left[ln\frac{AE_a}{R} + ln\frac{e^{-x}}{x^2} + lnh(x)\right] - ln(\beta) \tag{15}$$

Through the application of a linear regression of the least squares method and the plotting of ln g(α) against ln β, it is possible to ascertain that the slope of the straight line is –1.00000 and that the linear correlation coefficient R^2 is equivalent to unity. These results are contingent upon the investigated mechanism conforming to a particular $g(\alpha)$ function. Ascertained E_a and lnA values do not influence the shape of the most accurate reaction mechanism functions.

2.3.3 Thermodynamic calculations

The values of the thermodynamic parameters $\Delta S^{\#}$, $\Delta H^{\#}$, and $\Delta G^{\#}$ required to determine the formation of the activated complex from the reactants were calculated using the equations reported elsewhere.[5,38]

3 Results and discussion

3.1 Thermal decomposition of EuAc.xH$_2$O

Figure 1 compares the TG curves obtained by subjecting pristine and irradiated EuAc.xH2O in an air atmosphere to a temperature increase from room temperature to 900 °C.

Overall, the TG curve of EuAc.xH2O distinguished the following three principal decomposition steps I, II, and III:

3.1.1 Event-I (dehydration step)

This process occurs between 80 and 180 °C and is associated with the sequential depletion of water content. This step was accompanied by a single endothermic peak at 138 °C. The

Table 2: Summary of kinetic mechanism determinations.

Symbol	Reaction model	$y(\alpha)$	$z(\alpha)$
D_1	One dimensional diffusion	–	–
D_2	Two-dimensional diffusion (bidimentional particle shape) Valensi equation	Concave	0.834
D_3	Three-dimensional diffusion (tridimentional particle shape) Jander equation	Concave	0.704
JMA	Johnson Mehl Avram general equation (growth of nuclei)	$n(1-\alpha)[-\ln(1-\alpha)]^{1-1/n}$ n < 1: Concave n = 1:linear n > 1:0< α_m< α_p	0.632
R_2	Phase-boundary controlled reaction (contracting area, i.e., bidimensional shape)	Convex	0.750
R_3	Phase-boundary controlled reaction (contracting volume, i.e.,tridimensional shape)	Convex	0.704
SB(m,n)	Sestak-Berggren (Autocatalytic model)	$\alpha^m(1-\alpha)^n$ 0< α_m< α_p	Depending on exponents

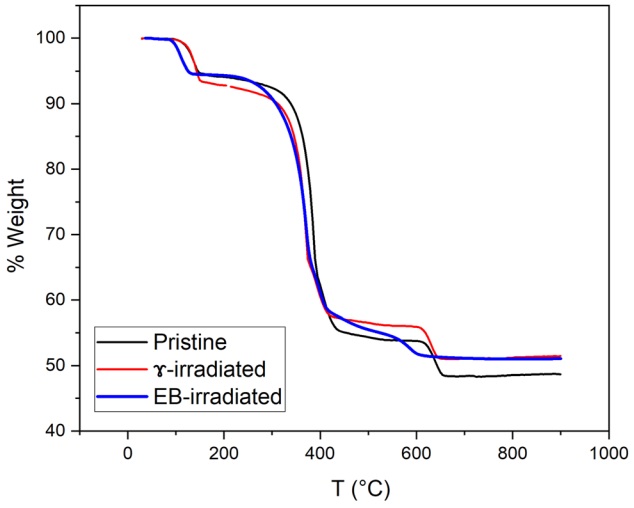

Figure 1: TG curves for the thermal decomposition of pristine as well as of gamma and electron-beam irradiated EuAc.xH_2O.

observed mass loss (ML) of 5.78 % is close to the theoretical value of 5.67 %.

In contrast to the irradiated samples of EuAc.xH_2O, the TG/DTG curves illustrate a nearly identical decomposition behavior. The endothermic peak associated with the dehydration step moves toward higher temperature ranges in *γ*-irradiated samples.

3.1.2 Event-II (release of acetate moieties)

The temperature range of 270–521 °C was determined to be conducive to the decomposition process, which was accompanied by the formation of an intermediate compound composed of $Eu_2O_2(CO_3)$ oxycarbonate and the liberation of three acetate moieties. The step was followed by two exothermic peaks with centers at 367.73 °C and 394.57 °C.

3.1.3 Event-III (formation of europium oxide)

A wide-ranging endothermic peak, with its center at 630 °C, was detected throughout this process, which transpired between 590 and 680 °C. The procedure entails the decomposition of $Eu_2O_2(CO_3)$ into a non-stoichiometric intermediate compound [$Eu_2O_{3-x}O$]. As calcination proceeds at 880 °C, this compound transforms into the pure phase of Eu_2O_3. The sum of the total mass losses (WL) is approximately 48.70 %, which is consistent with the 50.45 % of Eu_2O_3 residue remaining after decomposition. Compared with pristine sample, irradiated samples of EuAc.xH_2O, the TG/DTG curves display an increase in the decomposition percentage and a reduction in the induction period in the case of *γ* and EB, respectively.

Table 3: Thermal events for the dehydration of EuAc.xH_2O.

Sample type	Initial temperature T_i (°C)	Final temperature T_f (°C)	Max mass loss DTG_{max} (°C)
Pristine	89	161	109
γ-Irradiated	91	145	119
EB-irradiated	84	136	109

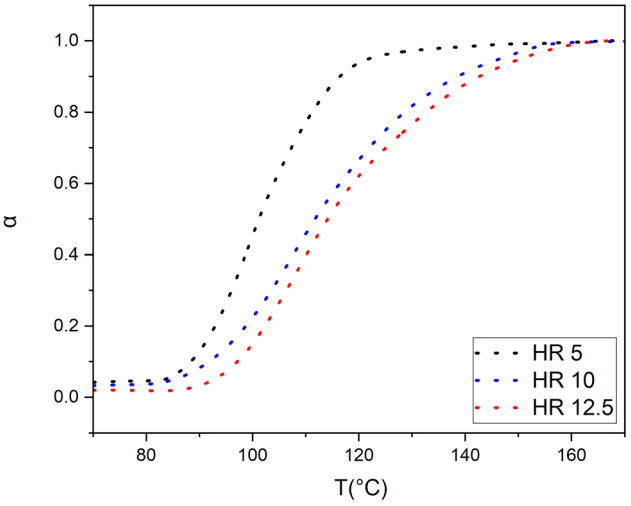

Figure 2: Variation of conversion degree, α, with temperature during non-isothermal dehydration of EuAc.xH_2O at the heating rates inserted in the figure.

Thermal events associated with the dehydration of pristine and irradiated samples of EuAc.xH_2O are listed in Table 3.

The conversion degree, α, versus T for EuAc.xH_2O at various heating rates (β), is illustrated in Figure 2. The results indicate that the α is contingent upon the particular heating rate chosen at a given temperature.

3.2 Analysis of the non-isothermal data

The activation energy values were computed using the FWO, KAS, Tang, Friedman, Iterative, and Vyazovkin methods and are presented in Table 4.

The E_α–α plot for the different linear isoconversional methods and the nonlinear *Vyazovkin* method are shown in Figure 3(a). The data illustrate a consistent pattern in the behavior between E_α and α, although different values are obtained when the *Friedman* equation is applied due to the linear and nonlinear methods used to approximate the temperature integral. It should be mentioned that the values of E_α obtained by nonlinear *Vyazovkin* are best fitted to *KAS* values, as indicated in Figure 3(a). The systematic decrease in

Table 4: Kinetic parameters (E_a(kJ/mol), ln$A(S^{-1})$) as a function of conversion degree, α, based on isoconversional methods for the non-isothermal dehydration of $EuAc.xH_2O$.

α	*FWO*			*KAS*			*Tang*			*Friedman*			*Iterative*			*Vyazovkin*		
	E_a	*ln* A	R^2	E_a	*ln* A	R^2	E_a	*ln* A	R^2	E_a	*ln* A	R^2	E_a	*ln* A	R^2	E_a	*ln* A	R^2
0.150	105.548	31.549	0.979	104.886	31.284	0.977	105.058	31.397	0.977	85.356	25.347	0.968	105.043	31.391	0.977	104.886	31.340	0.977
0.200	102.380	30.601	0.992	101.523	30.263	0.991	101.701	30.379	0.991	74.810	21.982	0.947	101.686	30.373	0.991	101.523	30.320	0.991
0.250	97.983	29.217	0.997	96.869	28.779	0.997	97.055	28.902	0.997	68.679	20.060	0.949	97.040	28.895	0.997	96.869	28.840	0.997
0.300	93.796	27.900	1.000	92.441	27.363	1.000	92.635	27.491	1.000	59.687	17.201	0.938	92.620	27.485	1.000	92.441	27.427	1.000
0.350	89.930	26.678	1.000	88.348	26.046	1.000	88.550	26.179	1.000	52.387	14.851	0.916	88.537	26.173	1.000	88.348	26.113	1.000
0.400	85.880	25.399	0.999	84.065	24.664	0.999	84.273	24.803	0.999	47.255	13.251	0.897	84.262	24.798	0.999	84.065	24.735	0.999
0.450	81.436	23.984	0.999	79.363	23.130	0.998	79.580	23.276	0.998	41.957	11.513	0.958	79.573	23.271	0.998	79.363	23.205	0.998
0.500	76.611	22.452	0.998	74.261	21.462	0.998	74.487	21.615	0.998	28.622	7.231	0.914	74.485	21.612	0.998	74.261	21.542	0.998
0.550	71.370	20.784	0.999	68.716	19.635	0.998	68.951	19.798	0.998	23.157	5.450	0.994	68.957	19.797	0.998	68.716	19.722	0.998
0.600	66.028	19.091	0.999	63.062	17.768	0.999	63.307	17.941	0.999	16.984	3.420	0.997	63.323	17.944	0.999	63.062	17.862	0.999
0.650	60.967	17.495	0.999	57.699	15.991	0.999	57.954	16.174	0.999	15.082	2.791	0.995	57.984	16.183	0.999	57.699	16.094	0.999
0.700	56.541	16.113	1.000	53.003	14.437	1.000	53.267	14.630	1.000	14.358	2.534	0.971	53.311	14.644	1.000	53.003	14.548	1.000
0.750	52.281	14.796	1.000	48.476	12.938	1.000	48.749	13.142	1.000	35.404	9.327	0.981	48.812	13.164	1.000	48.476	13.060	1.000
0.800	48.581	13.664	1.000	44.537	11.633	1.000	44.818	11.847	1.000	11.757	1.706	0.980	44.901	11.878	1.000	44.537	11.765	1.000
0.850	44.976	12.567	0.999	40.691	10.353	0.999	40.980	10.578	0.999	10.733	1.377	0.704	41.088	10.619	0.999	40.691	10.497	0.999
0.900	40.264	11.150	1.000	35.658	8.671	1.000	35.959	8.912	1.000	3.377	−0.950	0.988	36.106	8.971	1.000	35.658	8.835	1.000
Average	73.411	21.465	0.998	70.850	20.276	0.997	71.083	20.442	0.997	36.850 (35.659)*	9.818 (9.307)*	0.944	71.108	20.450	0.997	70.850	20.369	0.997
σ	21.390	6.723	0.005	22.664	7.422	0.006	22.623	7.382	0.006	25.519	8.209	0.071	22.577	7.365	0.006	22.664	7.390	0.006

The *ln A* value calculated using master-plot is 20.5 s^{-1}. *Data in parentheses are the parameters computed from predicted isothermal data.

the values of E_a by an increase in the conversion degree indicates that the dehydration process is controlled by one reaction mechanism.[39] The same trend was observed for the *lnA* – *α* plot as shown in Figure 3(b).

A correlation between *lnA* and E_a is not expected to exist in general; however, it does so in this specific case. The kinetics model is mathematically simplified by this correlation. As shown in Figure 4, we therefore plotted the *lnA* and E_a obtained from each method and observed a linear relationship between them.[40]

Application of *Kissinger* and *Ozawa–Flynn–Wall* using the values of T_{max} at different heating rates (equations (9) and (10)) are presented in Figure 5. E_a and *lnA* values obtained by these two methods gave comparable results with those obtained by isoconversional methods and the results are listed in Table 5.

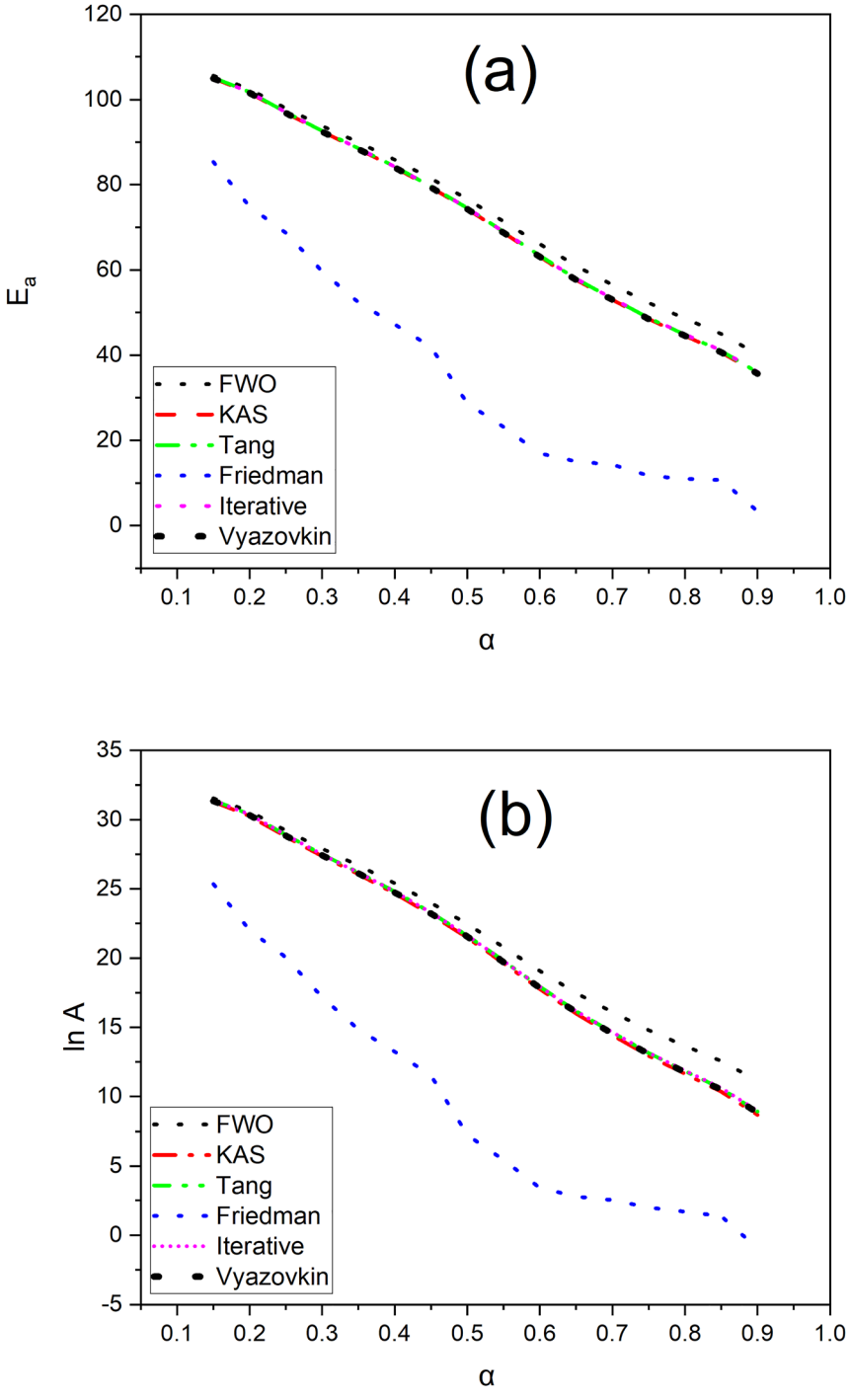

Figure 3: Dependencies of the activation energy, (a) E_a *(kJ/mol)* and (b) *ln A* (s^{-1}) on conversion degree, α, for non-isothermal dehydration of EuAc.xH_2O according to isoconversional methods.

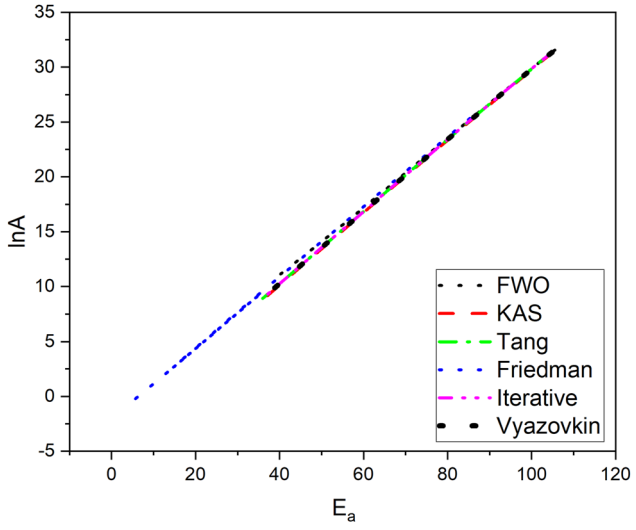

Figure 4: The relationship between *ln A(s^{-1})* and *E_a (kJ/mol)* in the dehydration process of EuAc.xH_2O using isoconversional methods.

3.3 Study of the thermal dehydration mechanism

Utilizing equation (11), analyzing non-isothermal data by the *master plots* method model R_2 served as an appropriate model for describing the reaction mechanism of the dehydration process with minimum values of the standard deviation as determined by equation (20). The findings are illustrated in Figure 6.

The introduction of the reaction model R_2 into equation (16) yields the equation (17):

$$g(\alpha) = \frac{AE_a}{\beta R}\int_x^\infty \frac{e^{-x}}{x^2}\,dx = \frac{AE_a}{\beta R}P(x) \tag{16}$$

$$1 - [(1-\alpha)]^{1/2} = \frac{AE_a}{\beta R}P(x) \tag{17}$$

The Arrhenius frequency factor (A) can be calculated by plotting the left-hand side of equation (17) against $E_aP(x)/\beta R$. The outcome is displayed in Figure 7, and the corresponding value of *lnA* is added to Table 4.

The variations of α versus T and dα/dt versus T for the thermal dehydration of EuAc.xH_2O are illustrated in Figure 8.

Málek equations (13) and (14) generated the experimental plots between normalized y(α) and α and normalized z(α) and α by utilizing the two plots. A summary of the mathematical properties of the y(α) and z(α) functions as they pertain to the fundamental kinetic models is presented in Table 2.

Figure 9 illustrates the variations of the normalized y(α) and z(α) functions on the conversion degree. The average E_a value of 35.66 kJ/mol, which was determined utilizing the *Friedman* method, was utilized in the calculation of the aforementioned functions (y(α) and z(α)). The variations of dα/dt versus α, y(α) versus α, and z(α) versus α are illustrated in Figure 9, where the heating rate is 5 °C/min. There are no significant differences observed in the experimental plots for the remaining two heating rates of 10 and 12.5 °C/min. Following this, the function of the most likely reaction mechanism for the dehydration process is established. The experimental data were described by the reaction mechanism function, which was calculated using the isoconversional Málek equations. The shape of z (α) is substantially identical for all heating rates and displays an average maximum of conversion at $\alpha_P^\infty \approx 0.750$ which coincides with the Masterplots R_2 model. The convex y (α) function of the R_2 model is also shown as inserted in Figure 9.

Equation (15) on the left-hand side was updated with the conversion degree (α) values corresponding to multiple rates measured at the same temperature after evaluating each of the mechanism functions listed in Table 1. Slope and correlation coefficient were calculated using the relationship between ln g(α) and ln β as the plot. The mechanism function with the highest correlation coefficient and the straight line slope value closest to –1.00000 was considered to be the most probable. Using the same methodology, the probable mechanism was determined using the values of conversion degree (α) that corresponded to multiple rates at the same temperature, provided that multiple g(α) functions met this criterion. Hence, the mechanism function was considered to be the most probable when the linear correlation coefficient R^2 approached unity and the slope of the straight line approached 1.00000.[23]

As shown in Table 6, the slope derived from the function of R_2 for the dehydration of pristine EuAc.xH_2O was the closest to –1.0000, and the correlation coefficient R^2 was superior. Therefore, it can be concluded that the function $g(\alpha) = [1-(1-\alpha)^{1/2}]$ in integral form and $f(\alpha) = 2(1-\alpha)^{1/2}$ in differential form are both components of the mechanism of phase boundary reaction. This function is highly likely to characterize the EuAc.xH_2O dehydration step.

3.4 Thermodynamic parameters

The thermodynamic parameters for the dehydration stage were computed utilizing the average activation energy and the pre-exponential factor. The results are given in Table 7. Based on the negative entropy value of the dehydration process, the reactant in the transition state, the activated compound, is more systematically arranged and possesses a reduced number of degrees of freedom concerning rotation

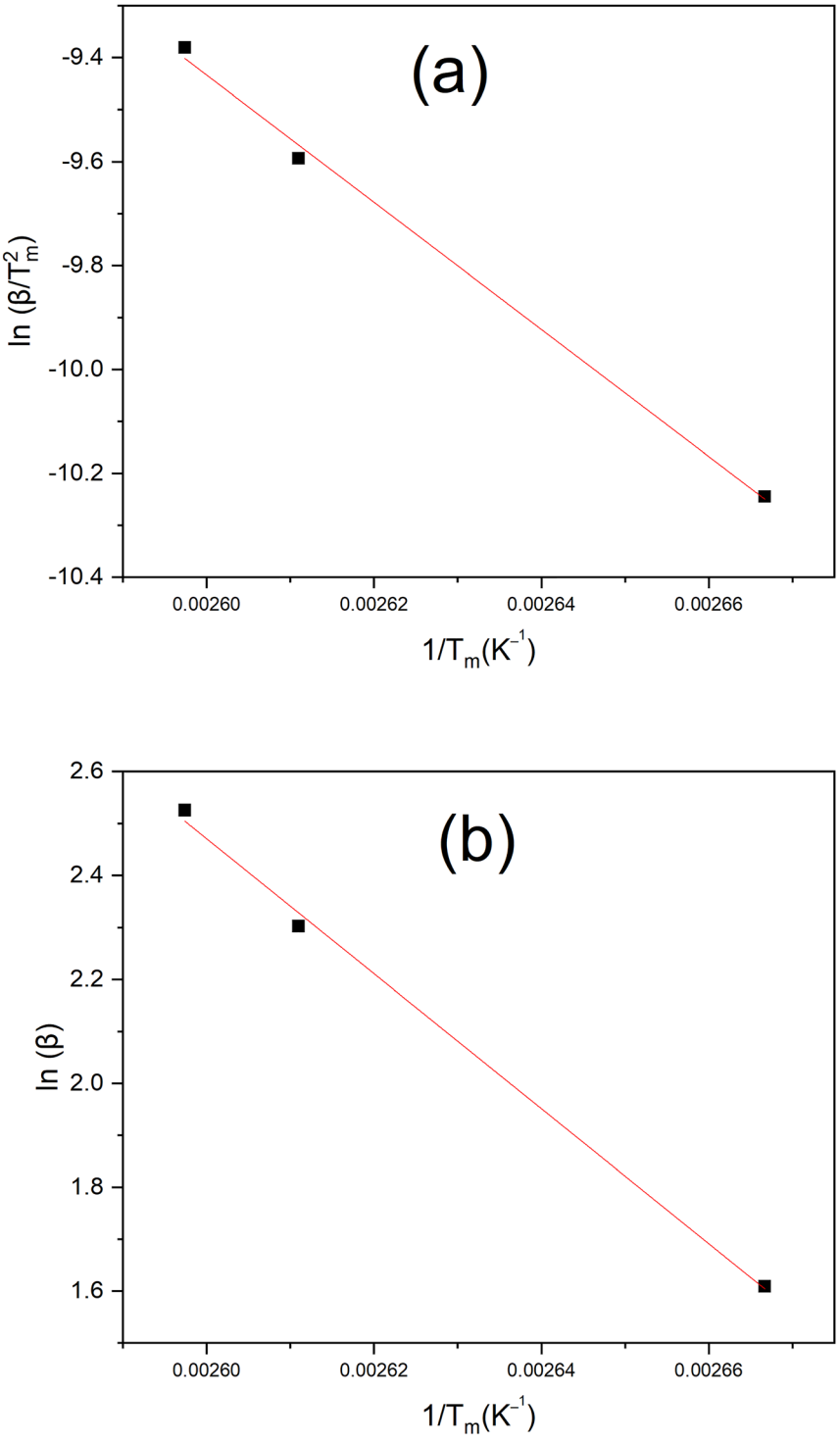

Figure 5: Kinetic parameters for thermal dehydration of EuAc.xH$_2$O (a) plot of *ln* (β/T_m^2) versus$1/T_m$ (Kissinger) and (b) plot of *ln* β versus $1/T_m$ (Ozawa).

Table 5: Kinetic parameters for thermal dehydration of EuAc.xH$_2$O.

Method	E_a (kJ mol^{-1})	*ln A* (S^{-1})	R^2
Kissinger	101.778	31.808	0.9972
Ozawa	102.748	45.696	0.9975

and vibration compared to the non-activated compound at the commencement of the dehydration process.[41] The positive values of $\Delta H^{\#}$ and $\Delta G^{\#}$ indicated that the dehydration process is non-spontaneous and is associated with heat absorption.

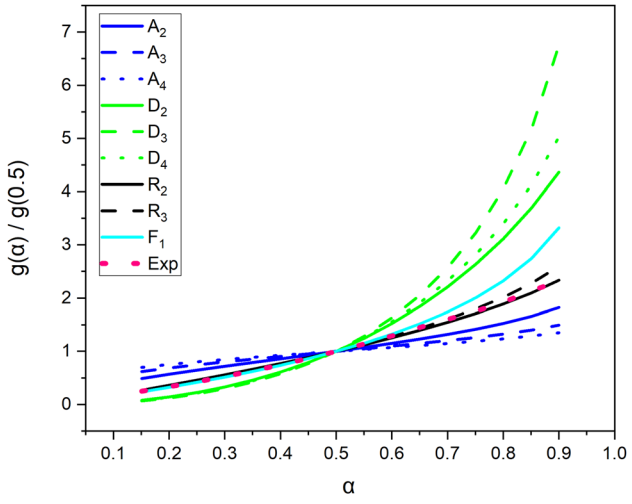

Figure 6: Theoretical and experimental master plots for the thermal dehydration of EuAc.xH$_2$O at the heating rates selected in this work. (See Table 1 for the abbreviations of the reaction models inserted in the figure).

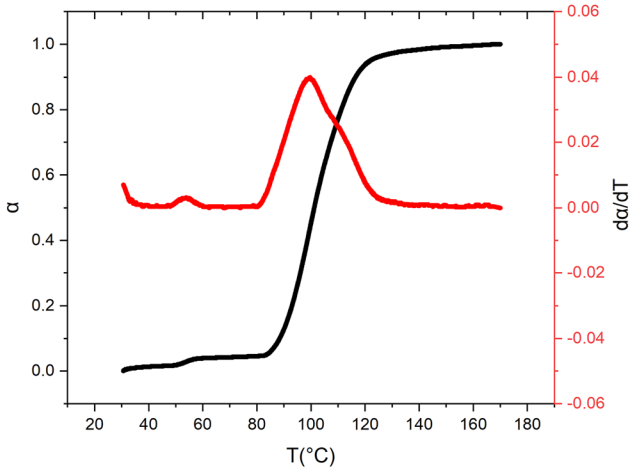

Figure 8: *α* versus T and dα/dT versus T for the thermal dehydration of EuAc.xH$_2$O at heating rate of 5 °C/min.

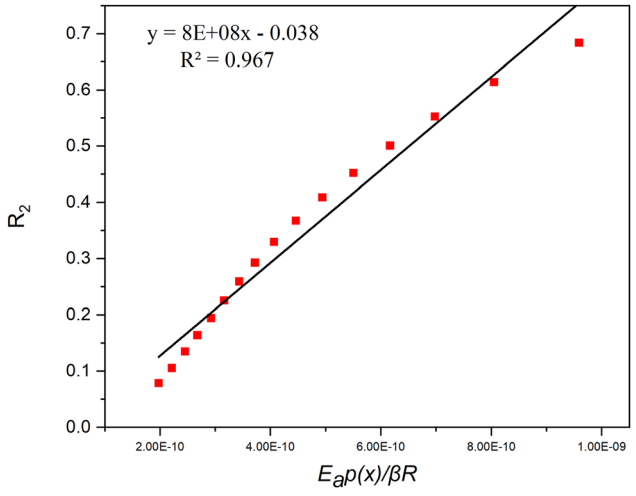

Figure 7: Determination of *A* value by plotting the selected reaction model against $E_aP(x)/\beta R$ for the thermal dehydration of EuAc.xH$_2$O at the heating rates applied in this work.

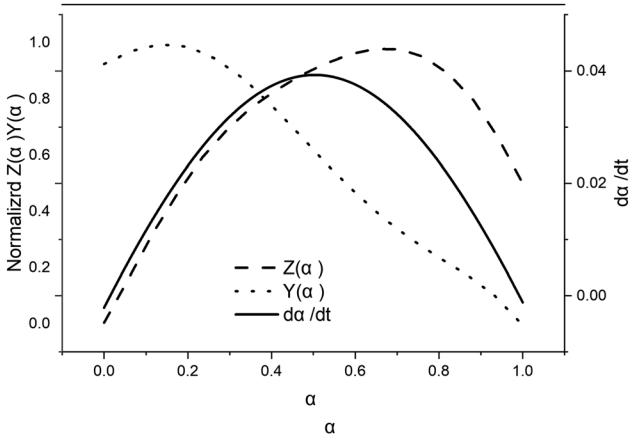

Figure 9: d*α*/d*t* versus *α*, *y*(*α*) versus *α*, and *z*(*α*) versus *α* plots for the thermal dehydration of EuAc.xH$_2$O at heating rate of 5 °C/min.

To assess the reliability of the estimated kinetic parameters derived from the employed techniques, the DTG curves utilizing the calculated kinetic parameters were plotted in Figure 10 and compared with experimental data collected at a heating rate of 5 °C/min^{-1} under non-isothermal conditions. The inability of the *Tang*, *FWO*, and *KAS* methods to produce a satisfactory match with the experimental DTG curve at a rate of 5 °C/min^{-1} is illustrated in Figure 10. On the contrary, the *Friedman* method produced reliable kinetic parameters for the dehydration step by exhibiting good agreements.

Table 6: The most probable mechanism function g(*α*), slope and the correlation coefficient of linear regression R^2 for different reaction models.

Reaction model	Slope	R^2
A2	−0.557	0.999
A3	−0.371	0.999
A4	−0.278	0.999
D2	−1.905	1.000
D3	−2.064	1.000
D4	−1.958	1.000
R2	−0.993	1.000
R3	−1.032	1.000
F1	−1.114	0.999

Table 7: Values of thermodynamic parameters for the thermal dehydration of EuAc.xH$_2$O.

$\Delta S^{\#}$ (kJ mol^{-1}K^{-1})	$\Delta H^{\#}$ (kJ mol^{-1})	$\Delta G^{\#}$ (kJ mol^{-1})
−0.089 (-0.180)[a]	67.471 (32.545)	100.401 (105.712)

[a]The thermodynamic data in parentheses are computed from predicted isothermal data.

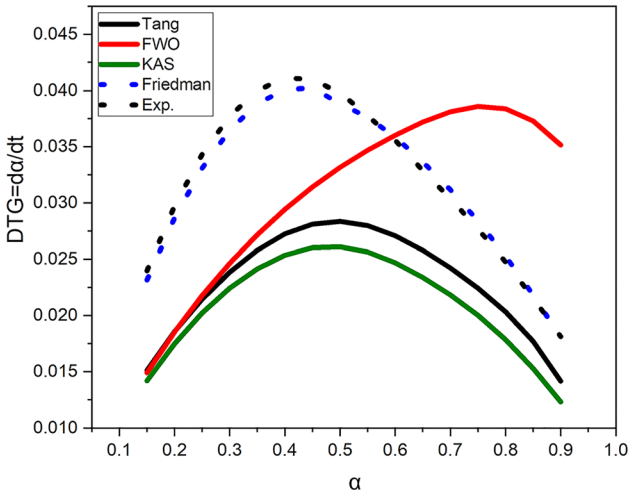

Figure 10: Non-isothermal DTG curves from the Friedman, Tang, FWO, KAS methods against the experimental data (β = 5 °C min^{-1}).

Figure 11 illustrates that the experimental and computed data were nearly identical, indicating that the kinetic triplets can reproduce and predict the thermal dehydration process of EuAc.xH$_2$O with high accuracy.

3.5 Prediction of isothermal kinetics

Equation (18) can be utilized to calculate the time at which the specified conversion will occur at an arbitrary temperature T_0, enabling the application of the model-free isoconversional approach developed by *Friedman* to forecast the isothermal conversion as a function of time beginning at any given temperature T_0.[42,43]

$$t_\alpha = \frac{\int_0^{T\alpha} \exp\left(\frac{-E_a}{RT}\right) dT}{\beta \exp\left(\frac{-E_a}{RT_0}\right)} \tag{18}$$

Where T_α is the temperature of the non-isothermal process at a given conversion degree *(α)*, with constant heating rate β and at a fixed temperature T_0. Equation (18) was applied to the dehydration decomposition to predict the isothermal conversion as a function of reaction time at four different temperatures, and the results are shown in Figure 12.

$$g_j(\alpha) = \int_0^{\alpha} \frac{d\alpha}{f(\alpha)} = k_j(T_i)t \tag{19}$$

The subscript j represents the selected reaction model. Substituting $g_j(\alpha) = R_2$ for the pristine sample and plotting $g_j(\alpha)$ versus t at the selected temperatures 360, 370, 380, and 390 K gave four straight lines, the slopes of which correspond to the rate constants (k_j). The findings are illustrated in Figure 13.

The rate constants at various temperatures T_i are calculated for a given reaction model, and the Arrhenius parameters are determined using equation (21).

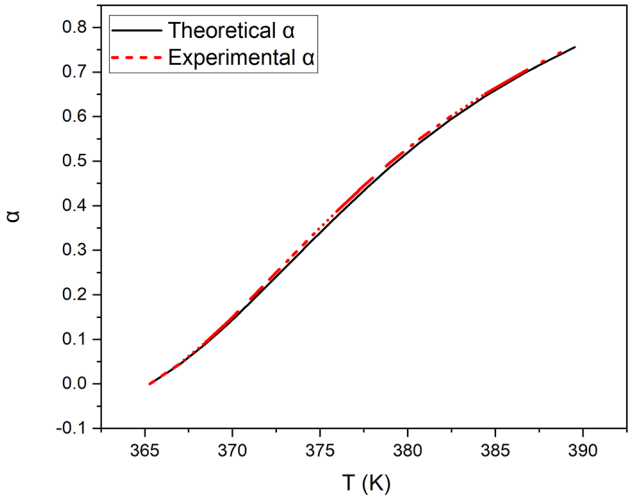

Figure 11: Computed and experimental *α* for the thermal dehydration of EuAc.xH$_2$O.

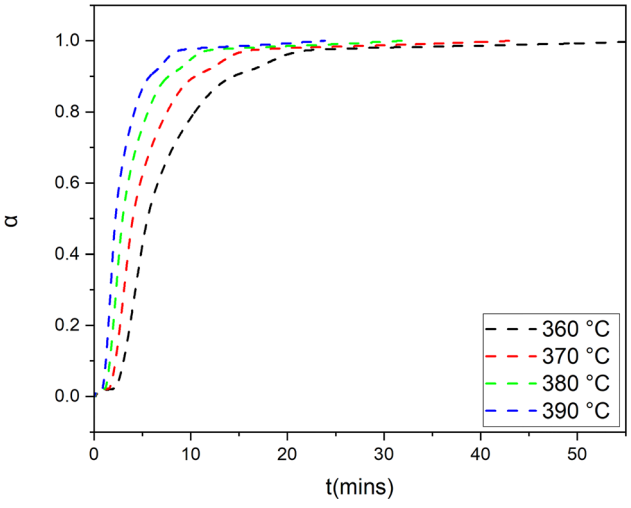

Figure 12: Predicted isothermal data (α vs. t) for the decomposition of EuAc.xH$_2$O at the temperature range of (360–390 °C).

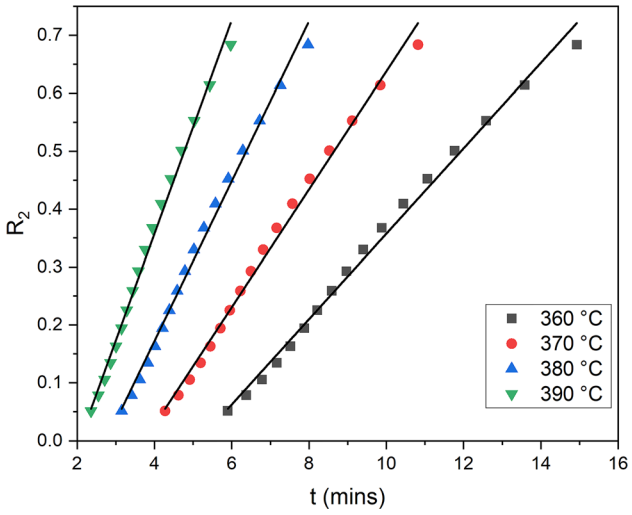

Figure 13: Kinetic analysis of the predicted isothermal data for the dehydration of EuAc.xH$_2$O at the temperature range of (360–390 °C).

$$\ln\left(k_j\left(T_i\right)\right) = \ln\left(k_{0j}\right) - \frac{E_{aj}}{RT_i} \tag{20}$$

$$\ln k_j = \ln A_j - \frac{E_{a,j}}{RT} \tag{21}$$

Plotting the left-hand side, which includes *ln k* versus *1/T*, gives E_a and *lnA* from the slope and intercept, respectively. The computed E_a and *lnA* parameters obtained from isothermal data were found to be in good agreement with those obtained from experimental non-isothermal data using the *Friedman* method (see Table 4). Once again, it could be emphasized that the *Friedman* method is the most reliable method to best fit the kinetic characteristic of the thermal dehydration process of EuAc.xH$_2$O.For the predicted isothermal decomposition, entropy and enthalpy values of the dehydration process were calculated using the following equation.

$$\ln\frac{k}{T} = -\frac{\Delta H^{\#}}{RT} + \ln\frac{R}{Nh} + \frac{\Delta S^{\#}}{R} \tag{22}$$

The slope and intercept of the function *ln k/T* versus *1/T* are denoted as $\Delta H^{\#}$ and $\Delta S^{\#}$, respectively, when *k* represents the rate constant, *R* signifies the gas constant, *T* represents the absolute temperature, *N* signifies Avogadro's number, and *h* signifies Planck's constant. The calculated values are in good agreement with the values obtained from the non-isothermal experiments .[44,45] The calculated thermodynamic parameters are also recorded in Table 7.

3.6 Further investigation of the dehydration process

The X-ray powder diffraction (P-XRD) technique was employed to evaluate the crystal structure of pristine as well as of gamma and electron beam (EB) irradiated samples of EuAc.xH$_2$O. XRD patterns of the three samples with different kinds of treatment display almost the same diffraction profiles. No changes in the position of the diffraction lines were detected by irradiation. Neither the disappearance of the diffraction lines nor the appearance of new diffraction lines were detected upon irradiation. A fullprof program was used to determine the crystallographic data of EuAc.xH$_2$O.[46] All the diffraction lines of the three investigated samples were indexes to the monoclinic system *(SG P2/m)*.

It is worth mentioning that the intensities of diffraction lines of *γ*-irradiated and EB- irradiated samples were higher than those reported for EuAc.xH$_2$O before radiation treatments. These results were in good agreement with the higher activation energy values of 120 and 113 kJ/mol reported for *γ*-irradiated and EB- irradiated samples, respectively, compared with the calculated activation energy value of the pristine sample (the results of the kinetic analysis of *γ*-irradiated and EB-irradiated samples will be published separately). Table 8 lists the obtained crystallographic data.

Figure 14 illustrates the IR spectra of pristine and irradiated EuAc.xH$_2$O. Irradiation did not induce the appearance of a new band or the disappearance of an existing one.

It should be mentioned that the decrease in the intensities of FT-IR bands assigned to water molecules for *γ*-irradiated and EB-irradiated samples was found to have lower intensities than the pristine sample. These results indicate that the samples' pre-irradiation led to the symmetrical orientation of the water molecules. This finding is in fair agreement with the data obtained from X-ray and kinetic calculations .[47]

Table 9 provides a list of the most major characteristic bands along with their respective assignments.

It is important to mention that the separation *Δν* between the symmetric and asymmetric frequencies of the COO^- group provides insight into the coordination characteristics of the COO^- anion with the lanthanide metal. The observed separations (*Δν*) in the EuAc.xH$_2$O samples under investigation fall within the range of 107–117 cm^{-1}, This result suggests the presence of the acetate anion as an unidentified ligand.[48]

4 Role of irradiation

The passage of charged particles EB and gamma ray (*γ*) through the sample may cause extensive ionization and electronic excitation, which in turn lead to bond rupture,

Table 8: Crystallographic data of EuAc.xH_2O.

Sample	Space group	*a* (Å)	*b*	*c*	*α*(°)	*β*	*γ*	System
Pristine	*P2/m*	16.21380	7.3864	11.8406	90.0000	105.1670	90.0000	Monoclinic
γ- irradiated	*P2/m*	16.34120	7.3964	11.8501	90.0000	105.1770	90.0000	Monoclinic
EB-irradiated	*P2/m*	16.32110	7.3952	11.8450	90.0000	105.1771	90.0000	Monoclinic

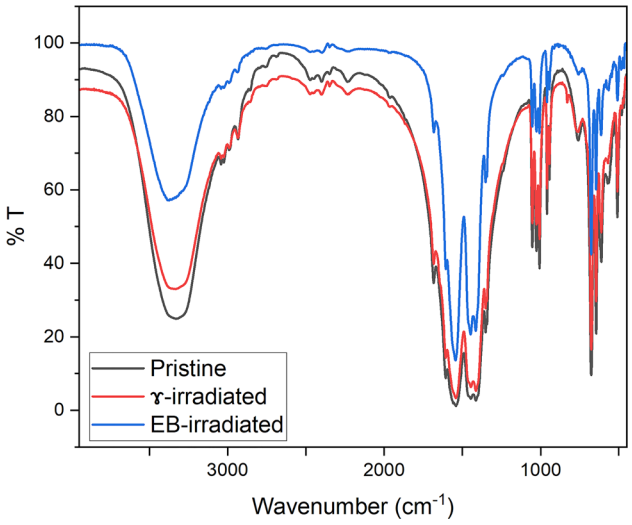

Figure 14: I.R. spectra of pristine as well as of gamma, and electron-beam irradiated EuAc.xH_2O.

Table 9: Some of the characteristic bands (cm^{-1}) recorded in the IR spectra of EuAc.xH_2O.

Pristine sample	γ- irradiated sample	EB- irradiated sample	Assignment
3,377	3,370	3,377	ν_{OH} asy.
3,285	3,278	3,300	ν_{OH} sy.
1,539	1,539	1,549	ν_{COO^-} asy.
1,432	1,432	1,432	ν_{COO^-} sy.
1,684	1,684	1,684	δ_{OH} bending
509	509	509	$\nu_{Eu\text{-}O}$

δ, Bending vibration; ν, Stretching; ν sy, Symmetric stretching; ν asy, Asymmetric stretching.

free radicals production, vacancies formation, and interstitial atoms. Compton scattering is the principal mode by which *γ*-rays interact with samples. Compton scattering has no significant effect on the lattice position of the Eu atom due to the high mass number of Eu (151.97). The formation of oxygen vacancies and the ionization process could lead to the observed increase in decomposition percentage and the reduction in the induction period in the case of gamma (*γ*) and EB interaction with the investigated sample, respectively.[49]

5 Conclusions

Through the use of both linear and nonlinear isoconversional techniques, europium (III) acetate hydrate was non-isothermal dehydrated in the air atmosphere. One step of dehydration produced 1.1 mol of crystalline water. When the non-isothermal dehydration data were analyzed using the *Master plots* method, it was determined that the phase boundary (R_2) controlled the kinetics of non-isothermal dehydration of pristine EuAc.xH_2O. TG/DTG curves of a pristine sample of EuAc.xH_2O were detectably altered by exposure to irradiation. The crystal system of pristine EuAc.xH_2O is monoclinic, and no change in the crystal system was detected upon irradiation. FTIR spectra showed a reduction in the functional bands' intensities, but neither the appearance of new bands nor the disappearance of old bands could be identified through irradiation. The dehydration processes are non-spontaneous and involve heat absorption, as indicated by the calculated thermodynamic parameters. A predicted thermogram (TG) of the isothermal decomposition of EuAc.xH_2O was constructed from non-isothermal data and used to discover the reaction model and the dehydration process kinetic parameters.

Acknowledgments: This work is part of Noura Saleh's Ph.D. thesis. The authors thank Assiut University for the official technical and financial support. The authors also would like to thank the crew team of radiation units at the Egyptian Atomic Energy Authority for facilitating the irradiation experiments.

Research ethics: Not applicable.

Informed consent: Informed consent was obtained from all individuals included in this study, or their legal guardians or wards.

Author contributions: The authors have accepted responsibility for the entire content of this manuscript and approved its submission.

Use of Large Language Models, AI and Machine Learning Tools: None declared.

Conflict of interest: The authors state no conflict of interest.

Research funding: The researchers extend appreciation to the Postgraduate Studies & Research Sector, Assiut University for funding this work as a research number: AUN2025F.Sci.H0004.
Data availability: Not applicable.

References

1. Mahfouz, R.; Al-Khamis, K. M.; Siddiqui, M.; Al-Hokbany, N.; Warad, I.; Al-Andis, N. Kinetic Studies of Isothermal Decomposition of Unirradiated and γ-irradiated Gallium Acetylacetonate: New Route for Synthesis of Gallium Oxide Nanoparticles. *Prog. React. Kinet. Mech.* **2012**, *37* (3), 249–262.
2. Mahfouz, R.; Ahmed, G.-W.; Alshammari, M. Application of the Model-free Approach to the Study of Non-isothermal Decomposition of Un-Irradiated and γ-Irradiated Hydrated Gadolinium Acetylacetonate. *Radiat. Eff. Defects Solids* **2014**, *169* (6), 490–498.
3. Mahfouz, R.; Monshi, M.; Abd El-Salam, N. Kinetics of the Thermal Decomposition of γ-Irradiated Gadolinium Acetate. *Thermochim. Acta* **2002**, *383* (1-2), 95–101.
4. Monshi, M.; Abd El-Salam, N.; Mahfouz, R. Gamma Irradiation Effects on the Thermal Decomposition Induction Period in Uranyl Acetate. *Thermochim. Acta* **1999**, *327* (1-2), 139–143.
5. Saleh, N. M.; Mahmoud, G. A.; Dahy, A. A.; Soliman, S. A.-F.; Mahfouz, R. M. Kinetics of Nonisothermal Dehydration of Unirradiated and γ-ray Irradiated Neodymium (III) Acetate Hydrate. *Radiochim. Acta* **2019**, *107* (2), 165–178.
6. Vyazovkin, S.; Wight, C. A. Model-free and Model-Fitting Approaches to Kinetic Analysis of Isothermal and Nonisothermal Data. *Thermochim. Acta* **1999**, *340*, 53–68.
7. Vyazovkin, S. Model-free Kinetics: Staying Free of Multiplying Entities without Necessity. *J. Therm. Anal. Calorim.* **2006**, *83* (1), 45–51.
8. Khawam, A.; Flanagan, D. R. Solid-state Kinetic Models: Basics and Mathematical Fundamentals. *J. Phy. Chem. B* **2006**, *110* (35), 17315–17328.
9. Vyazovkin, S.; Dollimore, D Linear and Nonlinear Procedures in Isoconversional Computations of the Activation Energy of Nonisothermal Reactions in Solids. *J. Chem. Inf. Comput. Sci.* **1996**, *36* (1), 42–45.
10. Farjas, J.; Roura, P. Isoconversional Analysis of Solid State Transformations: A Critical Review. Part I. Single Step Transformations with Constant Activation Energy. *J. Therm. Anal. Calorim.* **2011**, *105* (3), 757–766.
11. Hussein, G. A. Rare Earth Metal Oxides: Formation, Characterization and Catalytic Activity Thermoanalytical and Applied Pyrolysis Review. *J. Anal. Appl. Pyrolysis* **1996**, *37* (2), 111–149.
12. Spinks, J. W.; Woods, R. J. *An Introduction to Radiation Chemistry*, 3rd ed.; John Wiley & Sons: New York, 1990.
13. L'vov, B. V. *Thermal Decomposition of Solids and Melts: New Thermochemical Approach to the Mechanism, Kinetics and Methodology*; Springer Science & Business Media: Russian Federation, 2007.
14. Flynn, J. H; Wall, L. A. General Treatment of the Thermogravimetry of Polymers. *J. Res. Natl. Bur. Stand. Sec. A, Phy. Chem.* **1966**, *70* (6), 487.
15. Ozawa, T. A New Method of Analyzing Thermogravimetric Data. *Bull. Chem. Soc. Jpn.* **1965**, *38* (11), 1881–1886.
16. Kissinger, H. E. Reaction Kinetics in Differential Thermal Analysis. *Anal. Chem.* **1957**, *29* (11), 1702–1706.
17. Akahira, T.; Sunose, T. Method of Determining Activation Deterioration Constant of Electrical Insulating Materials. *Res Rep Chiba Inst Technol (Sci Technol)* **1971**, *16* (1971), 22–31.
18. Agrawal, R. K. Analysis of Non-isothermal Reaction Kinetics: Part 1. Simple Reactions. *Thermochim. Acta* **1992**, *203*, 93–110.
19. Tang, W.; Liu, Y.; Zhang, H; Wang, C. New Approximate Formula for Arrhenius Temperature Integral. *Thermochim. Acta* **2003**, *408* (1-2), 39–43.
20. Wanjun, T.; Yuwen, L.; Hen, Z; Zhiyong, W.; Cunxin, W. New Temperature Integral Approximate Formula for Non-isothermal Kinetic Analysis. *J. Therm. Anal. Calorim.* **2003**, *74* (1), 309–315.
21. Chunxiu, G.; Yufang, S.; Donghua, C. Comparative Method to Evaluate Reliable Kinetic Triplets of Thermal Decomposition Reactions. *J. Therm. Anal. Calorim.* **2004**, *76*, 203–216.
22. Liqing, L.; Donghua, C. Application of Iso-Temperature Method of Multiple Rate to Kinetic Analysis. *J. Therm. Anal. Calorim.* **2004**, *78* (1), 283–293.
23. Vlaev, L.; Nedelchev, N.; Gyurova, K.; Zagorcheva, M. A Comparative Study of Non-isothermal Kinetics of Decomposition of Calcium Oxalate Monohydrate. *J. Anal. Appl. Pyrolysis* **2008**, *81* (2), 253–262.
24. Senum, G.; Yang, R. Rational Approximations of the Integral of the Arrhenius Function. *J. Therm. Anal.* **1977**, *11* (3), 445–447.
25. Doyle, C. Estimating Isothermal Life from Thermogravimetric Data. *J. Appl. Polym. Sci.* **1962**, *6* (24), 639–642.
26. Coats, A. W.; Redfern, J. Kinetic Parameters from Thermogravimetric Data. *Nature* **1964**, *201* (4914), 68–69.
27. Shin, S.; Im, S. I.; Nho, N. S.; Lee, K. B. Kinetic Analysis Using Thermogravimetric Analysis for Nonisothermal Pyrolysis of Vacuum Residue. *J. Therm. Anal. Calorim.* **2016**, *126*, 933–941.
28. White, J. E.; Catallo, W. J.; Legendre, B. L. Biomass Pyrolysis Kinetics: a Comparative Critical Review with Relevant Agricultural Residue Case Studies. *J. Anal. Appl. Pyrolysis* **2011**, *91* (1), 1–33.
29. Sun, J.; Huang, Y.; Gong, G.; Cao, H Thermal Degradation Kinetics of Poly (Methylphenylsiloxane) Containing Methacryloyl Groups. *Polym. Degrad. Stab.* **2006**, *91* (2), 339–346.
30. Brown, M. E.; Galwey, A. K. The Significance of "Compensation Effects" Appearing in Data Published in "Computational Aspects of Kinetic Analysis": ICTAC Project, 2000. *Thermochim. Acta* **2002**, *387* (2), 173–183.
31. Flynn, J. H; Wall, L. A. A Quick, Direct Method for the Determination of Activation Energy from Thermogravimetric Data. *J. Polym. Sci. Part B: Polym. Let.* **1966**, *4* (5), 323–328.
32. Gotor, F. J.; Criado, J. M.; Malek, J.; Koga, N. Kinetic Analysis of Solid-State Reactions: the Universality of Master Plots for Analyzing Isothermal and Nonisothermal Experiments. *J. Phy. Chem. A* **2000**, *104* (46), 10777–10782.
33. Vyazovkin, S.; Burnham, A. K.; Criado, J. M.; Pérez-Maqueda, L. A.; Popescu, C.; Sbirrazzuoli, N. ICTAC Kinetics Committee Recommendations for Performing Kinetic Computations on Thermal Analysis Data. *Thermochim. Acta* **2011**, *520* (1-2), 1–19.
34. Málek, J. The Kinetic Analysis of Non-isothermal Data. *Thermochim. Acta* **1992**, *200*, 257–269.
35. Sronsri, C.; Noisong, P.; Danvirutai, C. Solid State Reaction Mechanisms of the LiMnPO4 Formation Using Special Function and Thermodynamic Studies. *Ind. Eng. Chem. Res.* **2015**, *54* (28), 7083–7093.
36. Málek, J. A Computer Program for Kinetic Analysis of Non-isothermal Thermoanalytical Data. *Thermochim. Acta* **1989**, *138* (2), 337–346.
37. Sronsri, C. Thermal Dehydration Kinetic Mechanism of Mn1. 8Co0. 1Mg0. 1P2O7· 2H2O Using Málek's Equations and Thermodynamic Functions Determination. *Trans. Nonferrous Metals Soc. China* **2018**, *28* (5), 1016–1026.

38. Barnes, P. Comprehensive Chemical Kinetics, Vol. 22. In *Reactions in the Solid State*; Bamford, C. H.; Tipper, C. F. H., Eds.; Elsevier: Amsterdam, 1980; p. 340.
39. Stankovic, B.; Jovanovic, J.; Adnadjevic, B. Application of the Suzuki–Fraser Function in Modelling the Non-isothermal Dehydroxylation Kinetics of Fullerol. *React. Kinet. Mech. Catal.* **2018**, *123*, 421–438.
40. Khedri, S.; Elyasi, S. Kinetic Analysis for Thermal Cracking of HDPE: A New Isoconversional Approach. *Polym. Degrad. Stab.* **2016**, *129*, 306–318.
41. Abu-Eittah, R.; Zaki, N.; Mohamed, M.; Kamel, L. Kinetics and Thermodynamic Parameters of the Thermal Decomposition of Bis (Imipraminium) Tetrachlorocuprate, Bis (Imipraminium) Tetrachloromercurate and Imipraminium Reineckate. *J. Anal. Appl. Pyrolysis* **2006**, *77* (1), 1–11.
42. Vyazovkin, S. A Unified Approach to Kinetic Processing of Nonisothermal Data. *Int. J. Chem. Kinet.* **1996**, *28* (2), 95–101.
43. Rashwan, N. F.; Wahid, H; Dahy, A. A.; Mahfouz, R. M. Thermal Decomposition of Un-irradiated and γ-ray Irradiated Holmium Acetate Tetrahydrate. Part 1: Kinetics of Nonisothermal Dehydration of Un-irradiated and γ-ray Irradiated Ho (CH3COO)3· 4H2O. *Radiochim. Acta* **2018**, *106* (9), 775–785.
44. Brown, M. E.; Dollimore, D; Galwey, A. K. *Reactions In the Solid State*; Elsevier: Amesterdam,Oxford,New York, 1980.
45. Eyring, H The Activated Complex in Chemical Reactions. *J. Chem. Phys.* **1935**, *3* (2), 107–115.
46. Rodríguez-Carvajal, J. Recent Advances in Magnetic Structure Determination by Neutron Powder Diffraction. *Phys. B* **1993**, *192* (1-2), 55–69.
47. Mahfouz, R.; Aly, A. A.; El-Meligy, A.; Zidan, A. Gamma Irradiation Effects on the Electric Conductivity Behaviour and IR Absorption Spectra of Some Haloacetato and Mixed Thiazoles-Haloacetato Transition Metal Complexes. *Isotopenpraxis Isot. Environ. Health Stud.* **1991**, *27* (5), 245–247.
48. Patil, K.; Chandrashekhar, G.; George, M. V.; Rao, C. N. R. Infrared Spectra and Thermal Decompositions of Metal Acetates and Dicarboxylates. *Can. J. Chem.* **1968**, *46* (2), 257–265.
49. Dienes, G.; Vineyard, G. *Radiation Effects in Solids*; Interscience Publ. Inc: New York, 1957.